THE JOURNAL OF PHYSICAL CHEMISTRY C
A JOURNAL OF THE AMERICAN CHEMICAL SOCIETY

pubs.acs.org/JPCC

Article

Selective Tandem CO_2-to-C_{2+} Alcohol Conversion at a Single-Crystal Au/Cu Bimetallic Interface

Published as part of The Journal of Physical Chemistry virtual special issue "Early-Career and Emerging Researchers in Physical Chemistry Volume 2".

Chenyuan Zhu,* Zhibin Zhang, Ruixi Qiao, Chunlei Yang, Siwen Zhao, Guoshuai Shi, Xinyang Gao, Huoliang Gu, Kaihui Liu, and Liming Zhang*

Cite This: *J. Phys. Chem. C* 2023, 127, 3470−3477

Read Online

ACCESS | Metrics & More | Article Recommendations | Supporting Information

ABSTRACT: Copper-based bimetallic heterostructures have recently gained extensive attention because of their promising capability to steer the selectivity of electrochemical CO_2 reduction into high-valued multicarbon products. However, a thorough mechanistic understanding toward the CO_2 reduction pathway and the influence of interfacial atomic configuration has not yet been unveiled. Herein, we rationally engaged facet engineering to construct a Au/Cu heterostructure *via* an epitaxial growth and observed that Au(110)/Cu(110) exhibited the highest yield rate toward multicarbon alcohols, compared with results for Au(111)/Cu(111) and Au(100)/Cu(100). According to electrochemical analysis, the enhanced activity was attributed to high-conversion capabilities of both CO_2-to-CO and *CO-to-C_{2+} alcohols. Moreover, we confirmed that the buildup of *CO is more crucial than the atomic arrangement of Cu surface for multicarbon production. Our work demonstrates a benchmark tandem CO_2 electroreduction system to explicitly link the interfacial atomic configuration to the electrocatalytic performance and sheds light on the facet engineering of bimetallic electrodes in electrolysis.

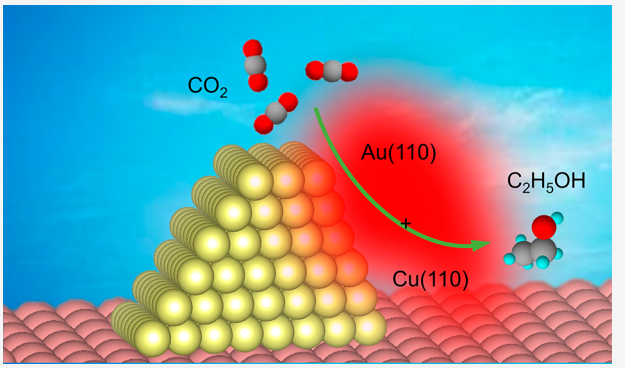

INTRODUCTION

The increase in the atmospheric CO_2 concentration has severely disturbed the balance of the natural carbon cycle, causing a variety of urgent environmental issues, such as global warming and ocean acidification.[1] Electrochemically converting CO_2 into fuels and chemicals powered by renewable energy represents a viable pathway to achieve carbon neutrality and lessen the heavy reliance on fossil fuels.[2,3] Distinct from hydrogen and oxygen evolution reactions, CO_2 reduction (CO_2R) can electrochemically generate various gaseous products (CO, CH_4, C_2H_4, *etc.*) and liquid products ($HCOO^-$, C_2H_5OH, *n*-C_3H_7OH, *etc.*). Among them, alcohols are highly desirable owing to their high energy densities and key role in the medical and food industries.[4−6] Cu is one of the foremost metals capable of driving CO_2 to multicarbon (C_{2+}) products with decent yields.[7,8] However, due to the complicated multiple electrons and sluggish proton-transfer kinetics, the direct conversion of CO_2 to C_{2+} alcohols at the Cu surface suffers from large overpotentials and low production rates.[9−11] Despite considerable efforts devoted to modifying the physical structures and/or chemical compositions of Cu catalysts, such as grain boundaries,[12] facets,[13,14] partially oxidized interface,[15,16] and alloying,[17] to improve the conversion of CO_2 to C_{2+} molecules, more facile strategies remain urgently needed in this research area.

Over the past few decades, the "tandem catalysis" strategy has been successfully demonstrated in thermal heterogeneous catalysis to control the selectivity in reaction networks.[18,19] Specifically, by rational surface engineering of the catalyst, the reaction rate of one step can be largely improved by judiciously increasing the coverage of one key intermediate, without strongly modulating the others. In Cu-based CO_2R, *CO (* denotes the surface adsorbed species) is proved to be critical for C_{2+} products.[20,21] Thereby, increasing the surface concentration of *CO and decoupling multiple steps of CO_2-to-C_{2+} to tandem CO_2-to-*CO and *CO-to-C_{2+} pathways is a promising strategy to increase the binding of *CO on Cu and thus improving the production of C_{2+} fuels on adjacent Cu surface *via* a spillover mechanism. Due to the strong

Received: November 24, 2022
Revised: January 31, 2023
Published: February 13, 2023

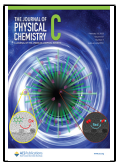

https://doi.org/10.1021/acs.jpcc.2c08241
J. Phys. Chem. C 2023, 127, 3470−3477

capability of reducing CO_2 to CO on the secondary metal (denoted as M, *e.g.*, Zn, Au, Ag, *etc.*),[22−25] the rational design of M/Cu heterostructures is commonly used to improve the activity and selectivity of C_{2+} products. Although the vital role of M/Cu has been experimentally shown, direct verification of the M/Cu interfacial structure and its influences on the production rate of C_{2+} products has not yet been demonstrated, which would highly hinder the related theoretical analysis and particularly impede the fundamental understanding of CO_2-to-C_{2+} conversion in tandem catalysis.

Au/Cu is a well-studied bimetallic heterostructure in tandem CO_2R system and can largely improve the production of C_{2+} products, especially C_{2+} alcohols, compared with results for Au, Cu, and AuCu alloy.[23,26] The present work aims to understand the facet-dependent C_{2+} alcohols production on Au/Cu bimetallic interface. We rationally designed and fabricated an epitaxial Au/Cu bimetallic heterostructure with different atomic orientations at the interface as a model system and revealed its intrinsic structure−function correlations for tandem CO_2R electrocatalysis. When tested for CO_2R, the Au(110)/Cu(110) heterostructure, relative to Au(111)/Cu(111) and Au(100)/Cu(100) counterparts, was confirmed to have a higher CO_2-to-CO conversion rate and an earlier onset for C_{2+} alcohols production, suggesting the crucial role of atomic arrangement at the bimetallic interface. The CO_2R pathway analysis further attributed the preference of C_{2+} alcohols production on Au(110)/Cu(110) to the simultaneously highest conversion capability of CO_2-to-CO and *CO-to-C_{2+} alcohols. We also confirmed that the buildup of *CO is more significant than the atomic arrangement of Cu surface for C_{2+} production in tandem catalysis. Overall, this work explicitly links the interfacial atomic configuration to the electrocatalytic performance in tandem CO_2R systems and reveals the importance of the facet engineering of bimetallic electrodes in electrolysis.

EXPERIMENTAL SECTION

Synthesis and Characterization of Epitaxial Au−Cu Bimetallic Heterostructures. The synthesis of single-crystal Au/Cu heterostructures refers to our previous work.[27,28] Specifically, the commercial Cu foil (25 μm thick, 99.8%, Sichuan Oriental Stars Trading Co. Ltd., #Cu-1031) was first loaded into a chemical vapor deposition furnace using a quartz substrate. After mild heating, the Cu foil was oxidized at 150−650 °C in air for 1−4 h. Afterward, the system was heated to 1020 °C in 1 h with 800 sccm Ar and 50 sccm H_2, then the Cu foil was annealed at 1020 °C for 3−10 h under the same atmosphere, and finally, the system was naturally cooled down to room temperature to obtain large-scale single-crystal Cu foils. The electron backscattered diffraction (EBSD) characterization was performed using a PHI 710 Scanning Auger Nanoprobe. The X-ray diffraction (XRD) of Cu foils was characterized by a Bruker D2 PHASER. X-ray photoelectron spectroscopy (XPS) (PHI 5000) measurements were employed using an Mg Ka source, with the pressure inside the chamber maintained below 4×10^{-9} Torr, and the spectra were collected at a pass energy of 17.9 eV. The highest peak in C 1s spectra was shifted to 284.8 eV for the charge correction. The scanning electron microscope coupled with energy dispersive spectroscopy (SEM-EDS, Nova NanoSem 450) was employed to analyze the surface morphologies and compositions of Au/Cu electrodes. The aberration-corrected high-angle annular dark field-scanning transmission electron microscopy (HADDF-STEM) characterization was performed on an FEI Titan Themis G2 300 operated at 300 kV.

Electrochemical CO_2R Measurement. Ambient pressure electrochemical CO_2 reduction was performed with a customized two compartment H-cell and an Biologic-SP300 potentiostat.[29] An anion exchange membrane (Fumatech company, Fumasep FAA-3-PK130) was used to separate the anodic and cathodic compartments, both of which were filled with CO_2-saturated 0.1 M $KHCO_3$ solution. Platinum foil and Ag/AgCl (CHI, 3 M KCl) were used as counter and reference electrodes, respectively. Potentials were converted to the RHE scale. The solution resistance was compensated for 85% by the potentiostat and the rest 15% was postcorrected. During electrolysis, CO_2 was constantly bubbled through the electrolyte with a flow rate of 5 sccm controlled by a mass flow-controller. One-hour chronoamperometry experiments were used to examine the activities of electrocatalysts across a broad range of potentials. The catalytic activities of gaseous and liquid products were quantified by an online gas chromatography (GC, Agilent 7890B) and 500 MHz ^{1}H nuclear magnetic resonance (NMR, AVANCE III HD) spectroscopy, respectively.

Product Analysis. The product analysis was performed according to our previous methods.[24] The error bars represent one standard deviation of triplicate measurements. Faradaic efficiencies (FEs) were calculated from the amount of charge passed to produce each product divided by the total charge passed at a specific time (gas products) or during the overall run (liquid products).

Calculation of the Faradaic Efficiency of gas products:

$$F.E.(gas) = \frac{F_{flow} \times (C_{gas}/V_m) \times n \times F}{I_{total} \times 60} \times 100$$

Calculation of the Faradaic Efficiency of liquid products:

$$F.E.(liqiud) = \frac{C_{liquid} \times V \times n \times F}{Q_{total}} \times 100$$

where

$F.E.$ (gas): Faradaic efficiency of gas product, %

$F.E.$ $(liquid)$: Faradaic efficiency of liquid product, %

F_{flow}: flow rate of CO_2, mL min^{-1}

C_{gas}: volume ratio of gas product, determined by online GC

V_m: the molar volume of an ideal gas at 1 atm of pressure (molar volume at *NTP* is 0.0245 mL), mL mol^{-1}

C_{liquid}: concentration of liquid product after 1 h of electrolysis, determined by NMR, mol L^{-1}

V: volume of the electrolyte in the working cell, L

I_{total}: steady-state cell current

Q_{total}: total charge in 1 h of bulk electrolysis, C

n: number of transferred electrons for certain product

F: Faradaic constant, 96485 C mol^{-1}

***In Situ* Raman Measurement.** The CO_2R on epitaxial Au/Cu electrodes was performed in a homemade H-type *in situ* Raman cell filled with CO_2-saturated 0.1 M $KHCO_3$ electrolyte, which was continuously flowed into the cell at a rate of 10 sccm. Meanwhile, the *in situ* Raman was applied to probe the reaction process. Raman spectra were taken by a Horiba HR800 system with a laser excitation energy of 638 nm. The laser spot size was 1 μm and a laser power of 5 mW was used to avoid heating.

https://doi.org/10.1021/acs.jpcc.2c08241
J. Phys. Chem. C 2023, 127, 3470−3477

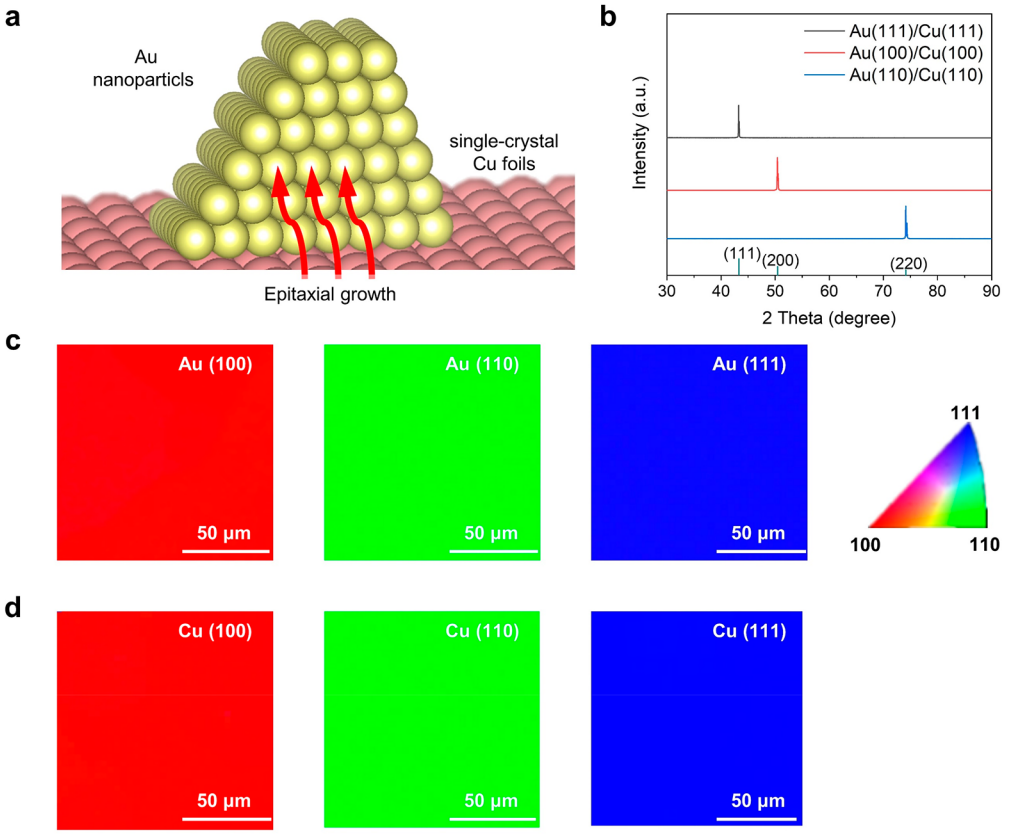

Figure 1. (a) A schematic illustration of as-prepared epitaxial Au/Cu heterostructure. (b) XRD 2 theta-scan of single-crystal Cu foils (PDF#04-0836). Large-scale EBSD mapping of the (c) single-crystal Au/Cu heterostructure and (d) single-crystal Cu.

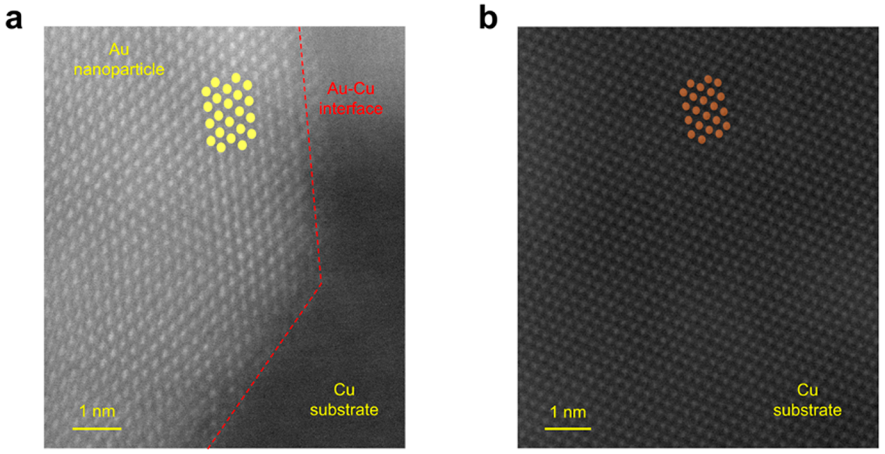

Figure 2. Atomically resolved STEM image of the Au(110)/Cu(110) interface: (a) Au(110) nanoparticle atop; (b) bottom Cu(110) substrate.

RESULTS AND DISCUSSION

Fabrication and Characterization of Single-Crystal Au/Cu Heterostructure. To elucidate the structure−function correlation, preparing the Au/Cu heterostructure with a well-defined interfacial atomic configuration is critical. As shown in Figure 1a, Au/Cu heterostructures were synthesized by epitaxially depositing the Au nanoparticles on Cu single-crystal foils. To confirm the formation of Au/Cu heterostructure, SEM-EDS and Auger mapping were conducted (Figures S1 and S2), which verified that Au was evenly distributed on Cu surface. The elemental contents were determined by XPS (Figure S3). Two symmetric peaks were observed in Au 4f spectra, having a binding energy of 87.8 ($4f_{5/2}$) and 84.2 ($4f_{7/2}$) eV, respectively, which suggested the valence state of Au was Au(0).[30] However, three subpeaks with binding energies of 932.3, 933.5, and 935.0 eV, respectively, could be deconvoluted in the Cu $2p_{3/2}$ spectra, which indicated the mixed valence states of Cu(II) and Cu(0). Cu(II) existed because an ultrathin CuO and/or $CuCO_3$ layer formed after exposing the electrode to air.[31] The XPS was used to identify the Au content on different single-crystal surfaces, which confirmed comparable Au/Cu surface ratios (Table S1). We further characterized the crystal orientation of Cu substrate using XRD. The sharp individual Cu(200), Cu(111), and Cu(220) peaks in 2θ scan with and without Au coverage confirmed that the growth of Au

https://doi.org/10.1021/acs.jpcc.2c08241
J. Phys. Chem. C 2023, 127, 3470−3477

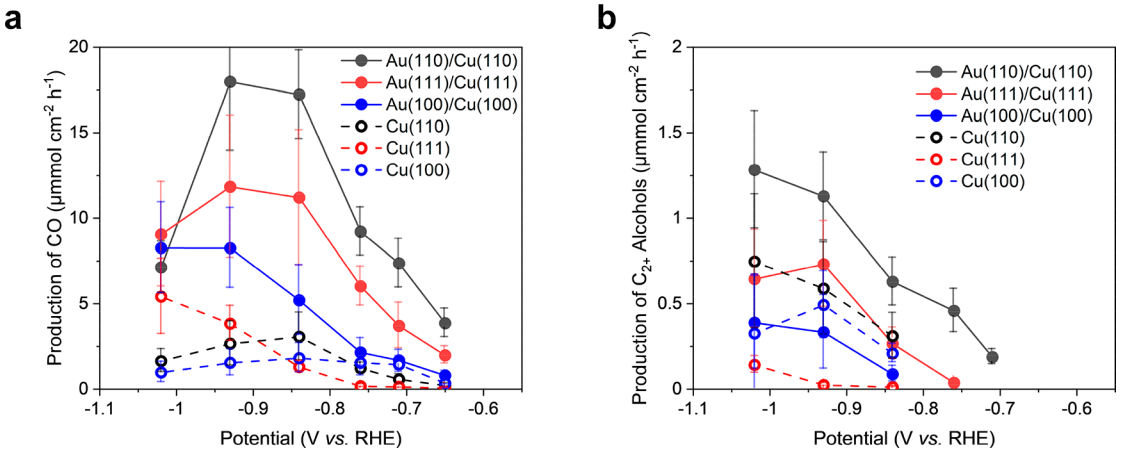

Figure 3. (a) Production rate of CO on Au/Cu and Cu electrodes. (b) Production rate of C_{2+} alcohols on Au/Cu and Cu electrodes.

nanoparticle barely influenced the orientation of Cu facets underneath (Figure 1b). In addition, no signals assignable to Au were observed in XRD due to the minor amount of Au deposited. To demonstrate the crystal orientation of both the Cu substrate and Au nanoparticle atop, EBSD was applied to analyze the crystal orientation. The uniform color contrast of EBSD verified the epitaxial growth of Au nanoparticles and the single-crystal nature of the bimetallic heterostructures, *e.g.*, the (100), (111), and (110) faceted Au nanoparticles on Cu(100), Cu(111), and Cu(110) substrates, respectively (Figure 1c,d).

Next, HAADF-STEM was implemented to investigate the Au/Cu interface at an atomic level. It reveals the smooth atomic boundary between Au and Cu (Figure 2a), wherein the atoms having a brighter contrast was assigned to Au due to its higher atomic number than Cu. The HAADF-STEM image was also collected on Cu substrate, revealing a uniform arrangement of Cu atoms (Figure 2b). We observed that the *out-of-plane* lattice fringes on Cu substrate and Au nanoparticles atop both exhibited typical *fcc* (110) planes, and the *in-plane* atomic arrangement revealed both (111) and (100) lattice constants (*e.g.*, Au(111), 2.37 Å; Au(100), 2.06 Å; Cu(111), 2.11 Å; Cu(100), 1.83 Å). All these characterizations demonstrated the successful epitaxial growth of Au nanoparticles on single-crystal Cu with a well-defined interfacial atomic configuration.

Electrochemical CO_2 Reduction Performance. The CO_2R performance of single-crystal Au/Cu was tested in a gastight two-compartment electrochemical cell with a CO_2-saturated 0.1 M $KHCO_3$ electrolyte and compared with those of bare single-crystal Cu facets. The electrochemical data at each potential, including J_{total}–V curves, FEs, and production rates for each product, were summarized in the Supporting Information (Figures S4–S6). The potential-dependent geometric current density at each voltage after an hour of electrolysis was recorded as shown in Figure S4, wherein the total current density increased with the negative potential on all three single-crystal Au/Cu electrodes. It was observed that Au(110)/Cu(110) displayed the highest current density under a lower overpotential; *e.g.*, at −0.75 V vs RHE, the total current density on Au(110)/Cu(110) was 1.5-fold and 2.5-fold higher than that on Au(111)/Cu(111) and Au(100)/Cu(100), respectively. At more negative potentials, the current density of Au(111)/Cu(111) gradually exceeded those of other two counterparts.

To probe the role of local *CO toward C_{2+} enhancement, the CO-producing rates on three single-crystal Au/Cu catalysts were first compared (Figure 3a). Previous reports have demonstrated that CO generation on Au outperforms Cu.[23,32] On the Au surface, CO_2 is mainly reduced to CO, which desorbs from the surface easily due to the unfavorable thermodynamics of Au for *CO adsorption. In contrast, CO binds stronger to the Cu surface (as *CO intermediates); thus, only a small CO flow can be detected. In our work, Au(110)/Cu(110) exhibited the highest CO selectivity (Figure 3a), likely due to the most unfavorable *CO adsorption capability of Au(110).[33] For example, in the potential window of −0.65 to −0.95 V vs RHE, Au(110)/Cu(110) showed a CO production rate nearly 2-fold higher than that of Au(111)/Cu(111), with a maximum value of 17.78 μmol cm^{-2} h^{-1} at −0.95 V vs RHE, indicating a high local *CO concentration near the Au(110)/Cu(110) interfacial perimeter. The CO-enriching capability of Au(110)/Cu(110) could be attributed to the highest electrochemical CO_2R kinetics of Au(110) among the low-index Au surfaces, consistent with the previous structural sensitivity study of single-crystal Au facets in the electrochemical conversion of CO_2 to CO.[33,34]

We next assessed the production rates of high-valued C_{2+} alcohols on three single-crystal Au/Cu. Benefiting from tandem catalysis, the CO_2-to-alcohols conversion rates on Au/Cu heterostructures were all significantly enhanced 1–2-fold in comparison with those of their monocrystalline Cu counterparts at −0.75 to −0.85 V vs RHE (Figure 3b), leading to the detection of alcohols at an onset potential 100–150 mV lower on Au/Cu heterostructures. Since the high-surface-area Au nanoclusters are unlikely to further convert CO to >2e^- products, the increased production of C_{2+} alcohols cannot be ascribed to the increased electrochemically active surface area (ECSA) resulting from Au. Moreover, we observed that the interfacial structure of Au/Cu critically influenced the production of C_{2+} alcohols. Au(110)/Cu(110) exhibited the highest alcohol production rate at a low overpotential (−0.75 V vs RHE), wherein the CO_2-to-alcohols conversion was 2- and 5-fold higher than those of Au(111)/Cu(111) and Au(100)/Cu(100), respectively. These differences were unlikely to result from the electrode surface roughness, as the ECSAs were observed to be similar on three Au/Cu heterostructures (Supplementary Figure S7 and Table S2). Instead, this improvement could be ascribed to the highest local *CO concentration at the epitaxial Au(110)/Cu(110)

https://doi.org/10.1021/acs.jpcc.2c08241
J. Phys. Chem. C 2023, 127, 3470–3477

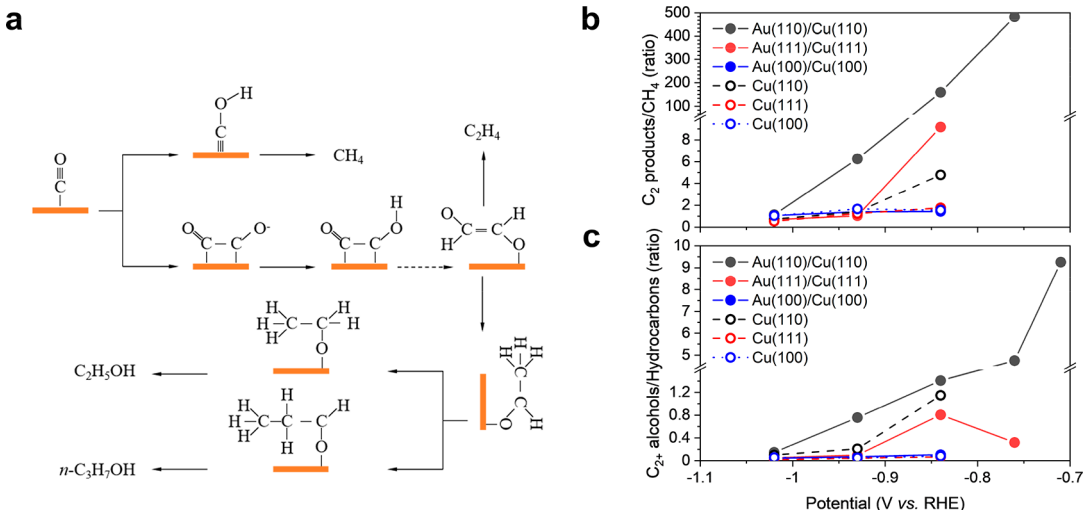

Figure 4. (a) The reaction pathway leading to specific CO_2 reduction products. Potential dependence of the molar ratio of (b) C_{2+} products to CH_4 and (c) C_{2+} alcohols to hydrocarbons on various single-crystal Au/Cu and Cu electrodes.

boundary (Figure 3a), which promoted the formation of C_{2+} alcohols on Cu(110) surface (Figure S5).

We also performed analysis on the generation rates of other >2e$^-$ products. Cu metal generally favors the production of hydrocarbons over the production of C_{2+} alcohols during CO_2R (Figure S5).[35,36] For instance, in our experiment, we observed that the production rates of CH_4 and C_2H_4 on Cu(100) and Cu(111) are both higher than the C_{2+} alcohols production rate across the potential window (Figure S6 and Figure 3b). However, in the Au/Cu tandem system, the production of hydrocarbons was strongly suppressed. For instance, after depositing Au nanoclusters on Cu(110), the production rate of C_2H_4 decreased from 0.14 to 0.04 μmol cm^{-2} h^{-1} at −0.85 V vs RHE, and the production of CH_4 was almost vanished (Figure S6). On the contrary, the production of C_{2+} alcohols on Au/Cu was largely promoted at a lower overpotential (Figure 3b), because the chemical C−C coupling on the Cu surface is more facile compared with electrochemical *CO to *CHO conversion under a low bias;[37] thus, the formation of C_2H_5OH is favored over C_2H_4.[38] Given that, Au(110)/Cu(110) can achieve the highest production of C_{2+} alcohols, and the various CO concentrations at differently faceted Au/Cu played a key role in modulating the production between hydrocarbons and C_{2+} alcohols.

To further elucidate the difference of *CO enrichment *in situ*, three single-crystal Au/Cu electrodes were mounted within a CO_2R electrochemical cell integrated with a confocal Raman microscope (Supplementary Figure S8). The Raman spectra exhibited peaks at 1380 and 1560 cm^{-1} at open circuit potentials (OCP), which were assigned to signals from (bi)carbonate species and water in the electrolyte, respectively.[39,40] Interestingly, after applying a bias of −0.2 V vs RHE, Au(110)/Cu(110) exhibited a unique peak at 2090 cm^{-1}, which could be assigned to the signal from C≡O stretching.[41] The absence of the C≡O signal on Au(111)/Cu(111) and Au(100)/Cu(100) was highly possible due to the much lower concentrations of *CO, which were under the detection limit of the Raman spectrometer. These observations are consistent with the different CO production rates shown in Figure 3a and reveal the importance of *in situ* production of *CO on Au/Cu heterostructures, which is critical to promote the tandem catalytic reduction of CO_2 to C_{2+} alcohols subsequently. These findings illustrate how tandem catalysis and structure-sensitive effects can be combined to tune the reaction pathway and product distribution of electrochemical CO_2R. We then compared the catalytic stabilities of Au(110)/Cu(110) and Au(111)/Cu(111) electrodes at −0.75 V vs RHE (Figure S9). Au(100)/Cu(100) was skipped here because it showed a much higher onset potential for C_{2+} alcohols. It was observed that both Au/Cu electrodes exhibited a stable current output and declined CO and C_{2+} alcohols production rates with time. Furthermore, Au(110)/Cu(110) showed a higher production rate stability than Au(111)/Cu(111), in which the yield of CO and C_{2+} alcohols dropped by ∼20% (from 7.92 to 6.28 μmol cm^{-2} h^{-1}) and ∼10% (from 0.36 to 0.32 μmol cm^{-2} h^{-1}) after 1 h electrocatalysis, respectively. In contrast, the CO and C_{2+} alcohols production on Au(111)/Cu(111) decreased ∼55% and ∼50%, respectively.

In addition, an important criterion for tandem CO_2R catalysis is the electrode composition durability under actual operating conditions. *Ex situ* XPS measurements on epitaxial Au(110)/Cu(110) evidenced that the surface content of Au dropped from 3.3 to 2.7 at. % after 1 h electrochemical testing, the decrease of which is much smaller than that of the Au/Cu heterostructure reported by Jaramillo *et al.* (from 10 to 0.4 at. %) after an identical experimental running (Supporting Information, Figure S10, and Table S3).[23] The evolution in the surface electrode composition may be attributed to a combination of particle detachment and surface modification on returning to the open circuit potential and being exposed to air. These results suggested that the epitaxial growth strategy provides a stronger interaction between Au and Cu and further increases the durability of the electrode in tandem CO_2R electrocatalysis. In addition to the Au content, the *ex situ* XPS determined the stable composition of Au/Cu surface after CO_2 reduction. As shown in Figure S10, the surface composition remained stable, and the valence state of Au remained Au(0). However, the XPS signal for Cu(II) vanished, indicating the unstable Cu(II) under the cathodic condition.

Pathway Analysis. To further understand the influences of the Au/Cu interface on the production of C_{2+} fuels, it is critical to understand the relationship between CO production, C−C dimerization, and tandem catalysis to C_{2+} products. As

https://doi.org/10.1021/acs.jpcc.2c08241
J. Phys. Chem. C 2023, 127, 3470−3477

summarized in Figure 4a, pathway diagrams were used to describe the entire CO_2R process based on one of the most recognized CO_2R roadmaps on Cu constructed by identifying some of key reaction intermediates.[42,43] Generally, the reduction of CO_2 starts with the hydrogenation of an adsorbed $*CO_2$ to form *COOH. After further reactions and OH desorption, the produced negatively charged *CO is a common precursor on the surface for the formation of following $>2e^-$ products. For CH_4, the key formyl (*CHO) serves as a selectivity-determining intermediate. The typical routes for C_{2+} products were also summarized, wherein the step that negatively charged $CO-CO^-$ species formed by *CO dimerization coupled with an electron transfer was identified as the rate-determining step (RDS). Thus, the competition between methanation and C−C coupling can be identified by examining the ratio of C_{2+} products to CH_4 as a function of potential (Figure 4b). The C_{2+}-to-CH_4 ratios for all three Au/Cu electrodes increased with the drop of an overpotential, indicating more positive potentials will benefit C−C coupling and suppress CH_4 formation. More importantly, the 4-fold higher C_{2+}-to-CH_4 ratio on an epitaxial Au(110)/Cu(110) catalyst is relative to the other two counterparts. Since the production of hydrocarbons (CH_4 + C_2H_4) followed competing production pathways with C_{2+} alcohols, we further calculated the mole ratio of C_{2+} alcohols to hydrocarbons to illustrate the facet-dependence of pathway competition. As shown in Figure 4c, this ratio increased dramatically with an overpotential dropping on Au/Cu electrodes, indicating C_{2+} alcohols are more preferable at the low potential range. Moreover, Au(110)/Cu(110) outperformed Au(111)/Cu(111) and Au(100)/Cu(100) to produce alcohols and suppress hydrocarbons, as demonstrated by the most positive onset potential and highest mole ratio at −0.75 V vs RHE. In addition, a significant amount of experimental and theoretical studies have demonstrated that the formation of C_{2+} products, especially C_2H_4, is much favored on Cu(100) over Cu(111). As shown in Figure 4b,c, it was observed that Au(111)/Cu(111) exhibited a higher C_{2+}/CH_4 and C_{2+} alcohols/hydrocarbons ratio than Au(100)/Cu(100), suggesting that, although Cu(100) provides more active sites for *CO to-C_{2+} conversion, the buildup of *CO determines the production rates of C_{2+} products. Therefore, we concluded that, for highly efficient C_{2+} production, the buildup of *CO is a priority relative to modifying solely the atomic arrangement of Cu.

CONCLUSION

To summarize, we demonstrated the interfacial atomic engineering of bimetallic heterostructure as a promising means to maximize the production of C_{2+} alcohols through tandem CO_2R electrocatalysis. In particular, single-crystal Au(110)/Cu(110) showed an earlier onset for C_{2+} alcohols production, a higher CO_2-to-C_{2+} alcohols conversion rate, and a higher selectivity for alcohols compared with the selectivities of its Au(111)/Cu(111) and Au(100)/Cu(100) counterparts, suggesting the crucial role of bimetallic atomic configuration. According to electrochemical analysis, the enhanced activity was attributed to the highest capability of both CO_2-to-CO and *CO-to-C_{2+} alcohols conversion. Moreover, we confirmed that the buildup of *CO determined the production rates of C_{2+} chemicals. Our work opens the door to elucidate the effects of facet engineering and promotes the activity and selectivity of Cu-based bimetallic heterostructure in CO_2 conversion to value-added fuels. The insight gained from such a single-crystal biphasic interface opens up new possibilities for developing highly active tandem catalysts.

ASSOCIATED CONTENT

Supporting Information

The Supporting Information is available free of charge at https://pubs.acs.org/doi/10.1021/acs.jpcc.2c08241.

Additional structural and spectroscopic characterizations of single-crystal Au/Cu heterostructures and electrochemical CO_2R analysis (SEM images, XPS and Raman spectra, electrochemical CO_2 reduction current density, FEs, production rates, scan rate vs. the average of cathodic and anodic current densities, current and production rates stability; tables of compositions and capacitance) (PDF)

AUTHOR INFORMATION

Corresponding Authors

Chenyuan Zhu − *Department of Chemistry, iChEM (Collaborative Innovation Center of Chemistry for Energy Materials) and Shanghai Key Laboratory of Molecular Catalysis and Innovative Materials, Fudan University, Shanghai 200438, China*; Email: chenyuanzhu@fudan.edu.cn

Liming Zhang − *Department of Chemistry, iChEM (Collaborative Innovation Center of Chemistry for Energy Materials) and Shanghai Key Laboratory of Molecular Catalysis and Innovative Materials, Fudan University, Shanghai 200438, China*; orcid.org/0000-0001-6795-3381; Email: zhanglm@fudan.edu.cn

Authors

Zhibin Zhang − *State Key Laboratory for Mesoscopic Physics, Frontiers Science Center for Nano-optoelectronics, School of Physics, Peking University, Beijing 100871, China*

Ruixi Qiao − *Institute for Frontier Science, Nanjing University of Aeronautics and Astronautics, Nanjing 210016, China*

Chunlei Yang − *Department of Chemistry, iChEM (Collaborative Innovation Center of Chemistry for Energy Materials) and Shanghai Key Laboratory of Molecular Catalysis and Innovative Materials, Fudan University, Shanghai 200438, China*

Siwen Zhao − *Department of Chemistry, iChEM (Collaborative Innovation Center of Chemistry for Energy Materials) and Shanghai Key Laboratory of Molecular Catalysis and Innovative Materials, Fudan University, Shanghai 200438, China*

Guoshuai Shi − *Department of Chemistry, iChEM (Collaborative Innovation Center of Chemistry for Energy Materials) and Shanghai Key Laboratory of Molecular Catalysis and Innovative Materials, Fudan University, Shanghai 200438, China*

Xinyang Gao − *Department of Chemistry, iChEM (Collaborative Innovation Center of Chemistry for Energy Materials) and Shanghai Key Laboratory of Molecular Catalysis and Innovative Materials, Fudan University, Shanghai 200438, China*

Huoliang Gu − *Department of Chemistry, iChEM (Collaborative Innovation Center of Chemistry for Energy Materials) and Shanghai Key Laboratory of Molecular Catalysis and Innovative Materials, Fudan University, Shanghai 200438, China*

Kaihui Liu − *State Key Laboratory for Mesoscopic Physics, Frontiers Science Center for Nano-optoelectronics, School of Physics, Peking University, Beijing 100871, China;* orcid.org/0000-0002-8781-2495

Complete contact information is available at: https://pubs.acs.org/10.1021/acs.jpcc.2c08241

Notes

The authors declare no competing financial interest.

■ ACKNOWLEDGMENTS

This work is funded by the Natural Science Foundation of China (Grants 21872039, 22072030 and 22272029), Science and Technology Commission of Shanghai Municipality (Grants 18JC1411700, 19DZ2270100, and 22520711100), and the Fundamental Research Funds for the Central Universities (20720220008).

■ REFERENCES

(1) Cavicchioli, R.; Ripple, W. J.; Timmis, K. N.; Azam, F.; Bakken, L. R.; Baylis, M.; Behrenfeld, M. J.; Boetius, A.; Boyd, P. W.; Classen, A. T.; et al. Scientists' warning to humanity: microorganisms and climate change. *Nat. Rev. Microbiol.* **2019**, *17*, 569−586.

(2) Montoya, J. H.; Seitz, L. C.; Chakthranont, P.; Vojvodic, A.; Jaramillo, T. F.; Nørskov, J. K. Materials for solar fuels and chemicals. *Nat. Mater.* **2017**, *16*, 70−81.

(3) Ross, M. B.; De Luna, P.; Li, Y.; Dinh, C.-T.; Kim, D.; Yang, P.; Sargent, E. H. Designing materials for electrochemical carbon dioxide recycling. *Nat. Catal.* **2019**, *2*, 648−658.

(4) Nitopi, S.; Bertheussen, E.; Scott, S. B.; Liu, X.; Engstfeld, A. K.; Horch, S.; Seger, B.; Stephens, I. E. L.; Chan, K.; Hahn, C.; et al. Progress and Perspectives of Electrochemical CO2 Reduction on Copper in Aqueous Electrolyte. *Chem. Rev.* **2019**, *119*, 7610−7672.

(5) Birdja, Y. Y.; Pérez-Gallent, E.; Figueiredo, M. C.; Göttle, A. J.; Calle-Vallejo, F.; Koper, M. T. M. Advances and challenges in understanding the electrocatalytic conversion of carbon dioxide to fuels. *Nat. Energy* **2019**, *4*, 732−745.

(6) Arán-Ais, R. M.; Gao, D.; Roldan Cuenya, B. Structure- and Electrolyte-Sensitivity in CO2 Electroreduction. *Acc. Chem. Res.* **2018**, *51*, 2906−2917.

(7) Gao, D.; Arán-Ais, R. M.; Jeon, H. S.; Roldan Cuenya, B. Rational catalyst and electrolyte design for CO2 electroreduction towards multicarbon products. *Nat. Catal.* **2019**, *2*, 198−210.

(8) Hori, Y.; Kikuchi, K.; Suzuki, S. J. C. L. Production of CO and CH_4 in electrochemical reduction of CO2 at metal electrodes in aqueous hydrogencarbonate solution. *Chem. Lett.* **1985**, *14*, 1695−1698.

(9) She, X.; Wang, Y.; Xu, H.; Chi Edman Tsang, S.; Ping Lau, S. Challenges and Opportunities in Electrocatalytic CO_2 Reduction to Chemicals and Fuels. *Angew. Chem., Int. Ed.* **2022**, *61* (49), e202211396.

(10) Yang, Y.; Zhang, Y.; Hu, J. S.; Wan, L. J. Progress in the Mechanisms and Materials for CO_2 Electroreduction toward C_{2+} Products. *Acta Phys. Chim. Sin* **2020**, *36*, 1906085.

(11) Meng, Y.; Kuang, S.; Liu, H.; Fan, Q.; Ma, X.; Zhang, S. Recent advances in electrochemical CO_2 reduction using copper-based catalysts. *Acta Phys. Chim. Sin* **2021**, *37* (5), 2006034.

(12) Wu, Z.-Z.; Zhang, X.-L.; Niu, Z.-Z.; Gao, F.-Y.; Yang, P.-P.; Chi, L.-P.; Shi, L.; Wei, W.-S.; Liu, R.; Chen, Z.; Hu, S.; Zheng, X.; Gao, M.-R. Identification of Cu(100)/Cu(111) Interfaces as Superior Active Sites for CO Dimerization During CO_2 Electroreduction. *J. Am. Chem. Soc.* **2022**, *144*, 259−269.

(13) Li, H.; Yu, P.; Lei, R.; Yang, F.; Wen, P.; Ma, X.; Zeng, G.; Guo, J.; Toma, F. M.; Qiu, Y.; et al. Facet-Selective Deposition of Ultrathin Al_2O_3 on Copper Nanocrystals for Highly Stable CO_2 Electroreduction to Ethylene. *Angew. Chem., Int. Ed.* **2021**, *60*, 24838−24843.

(14) Zhu, C.; Zhang, Z.; Zhong, L.; Hsu, C.-S.; Xu, X.; Li, Y.; Zhao, S.; Chen, S.; Yu, J.; Chen, S.; et al. Product-specific active site motifs of Cu for electrochemical CO_2 reduction. *Chem.* **2021**, *7*, 406−420.

(15) Lyu, Z.; Zhu, S.; Xie, M.; Zhang, Y.; Chen, Z.; Chen, R.; Tian, M.; Chi, M.; Shao, M.; Xia, Y. Controlling the Surface Oxidation of Cu Nanowires Improves Their Catalytic Selectivity and Stability toward C_{2+} Products in CO_2 Reduction. *Angew. Chem., Int. Ed.* **2021**, *60*, 1909−1915.

(16) Lei, Q.; Zhu, H.; Song, K.; Wei, N.; Liu, L.; Zhang, D.; Yin, J.; Dong, X.; Yao, K.; Wang, N.; Li, X.; et al. Investigating the Origin of Enhanced C_{2+} Selectivity in Oxide-/Hydroxide-Derived Copper Electrodes during CO_2 Electroreduction. *J. Am. Chem. Soc.* **2020**, *142*, 4213−4222.

(17) Ma, S.; Sadakiyo, M.; Heima, M.; Luo, R.; Haasch, R. T.; Gold, J. I.; Yamauchi, M.; Kenis, P. J. A. Electroreduction of Carbon Dioxide to Hydrocarbons Using Bimetallic Cu−Pd Catalysts with Different Mixing Patterns. *J. Am. Chem. Soc.* **2017**, *139*, 47−50.

(18) Yan, H.; He, K.; Samek, I. A.; Jing, D.; Nanda, M. G.; Stair, P. C.; Notestein, J. M. J. S. Tandem In2O3-Pt/Al2O3 catalyst for coupling of propane dehydrogenation to selective H_2 combustion. *Science* **2021**, *371*, 1257−1260.

(19) Lian, J.-J.; Lin, C.-C.; Chang, H.-K.; Chen, P.-C.; Liu, R.-S. Thermal and Metal-Catalyzed Cyclization of 1-Substituted 3,5-Dien-1-ynes via a [1,7]-Hydrogen Shift: Development of a Tandem Aldol Condensation−Dehydration and Aromatization Catalysis between 3-En-1-yn-5-al Units and Cyclic Ketones. *J. Am. Chem. Soc.* **2006**, *128*, 9661−9667.

(20) Schouten, K. J. P.; Qin, Z.; Pérez Gallent, E.; Koper, M. T. M. Two Pathways for the Formation of Ethylene in CO Reduction on Single-Crystal Copper Electrodes. *J. Am. Chem. Soc.* **2012**, *134*, 9864−9867.

(21) Huang, Y.; Handoko, A. D.; Hirunsit, P.; Yeo, B. S. Electrochemical Reduction of CO2 Using Copper Single-Crystal Surfaces: Effects of CO* Coverage on the Selective Formation of Ethylene. *ACS Catal.* **2017**, *7*, 1749−1756.

(22) Ren, D.; Gao, J.; Pan, L.; Wang, Z.; Luo, J.; Zakeeruddin, S. M.; Hagfeldt, A.; Grätzel, M. Atomic Layer Deposition of ZnO on CuO Enables Selective and Efficient Electroreduction of Carbon Dioxide to Liquid Fuels. *Angew. Chem., Int. Ed.* **2019**, *58*, 15036−15040.

(23) Morales-Guio, C. G.; Cave, E. R.; Nitopi, S. A.; Feaster, J. T.; Wang, L.; Kuhl, K. P.; Jackson, A.; Johnson, N. C.; Abram, D. N.; Hatsukade, T.; Hahn, C.; Jaramillo, T. F. Improved CO_2 reduction activity towards C_{2+} alcohols on a tandem gold on copper electrocatalyst. *Nat. Catal.* **2018**, *1*, 764−771.

(24) Huang, J.; Mensi, M.; Oveisi, E.; Mantella, V.; Buonsanti, R. Structural Sensitivities in Bimetallic Catalysts for Electrochemical CO_2 Reduction Revealed by Ag−Cu Nanodimers. *J. Am. Chem. Soc.* **2019**, *141*, 2490−2499.

(25) Chen, C.; Li, Y.; Yu, S.; Louisia, S.; Jin, J.; Li, M.; Ross, M. B.; Yang, P. Cu-Ag tandem catalysts for high-rate CO_2 electrolysis toward multicarbons. *Joule* **2020**, *4*, 1688−1699.

(26) Kim, D.; Xie, C.; Becknell, N.; Yu, Y.; Karamad, M.; Chan, K.; Crumlin, E. J.; Nørskov, J. K.; Yang, P. Electrochemical Activation of CO_2 through Atomic Ordering Transformations of AuCu Nanoparticles. *J. Am. Chem. Soc.* **2017**, *139*, 8329−8336.

(27) Wu, M.; Zhang, Z.; Xu, X.; Zhang, Z.; Duan, Y.; Dong, J.; Qiao, R.; You, S.; Wang, L.; Qi, J.; Zou, D.; Shang, N.; Yang, Y.; Li, H.; Zhu, L.; Sun, J.; Yu, H.; Gao, P.; Bai, X.; Jiang, Y.; Wang, Z.-J.; Ding, F.; Yu, D.; Wang, E.; Liu, K. Seeded growth of large single-crystal copper foils with high-index facets. *Nature* **2020**, *581*, 406−410.

(28) Zhu, C.; Zhou, L.; Zhang, Z.; Yang, C.; Shi, G.; Zhao, S.; Gu, H.; Wu, J.; Gao, X.; Li, Y. J. C. Dynamic restructuring of epitaxial Au−Cu biphasic interface for tandem CO_2-to-C_{2+} alcohols conversion. *Chem.* **2022**, *8*, 3288−3301.

(29) Zhu, C.; Zhang, Z.; Zhong, L.; Zhao, S.; Shi, G.; Wu, B.; Gu, H.; Wu, J.; Gao, X.; Liu, K.; et al. Enhanced electrochemical CO_2-to-C_{2+} conversion from synergistic interaction between terrace and step sites on monocrystalline high-index Cu facets. *J. Energy Chem.* **2022**, *70*, 382−387.

(30) Jia, H.; Yang, Y.; Chow, T. H.; Zhang, H.; Liu, X.; Wang, J.; Zhang, C.-Y. Symmetry-Broken Au−Cu Heterostructures and their Tandem Catalysis Process in Electrochemical CO_2 Reduction. *Adv. Funct. Mater.* **2021**, *31*, 2101255.
(31) Li, C. W.; Kanan, M. W. CO_2 Reduction at Low Overpotential on Cu Electrodes Resulting from the Reduction of Thick Cu_2O Films. *J. Am. Chem. Soc.* **2012**, *134*, 7231−7234.
(32) Shi, C.; Chan, K.; Yoo, J. S.; Nørskov, J. K. Barriers of Electrochemical CO_2 Reduction on Transition Metals. *Org. Process Res. Dev.* **2016**, *20*, 1424−1430.
(33) Todoroki, N.; Tei, H.; Tsurumaki, H.; Miyakawa, T.; Inoue, T.; Wadayama, T. Surface Atomic Arrangement Dependence of Electrochemical CO_2 Reduction on Gold: Online Electrochemical Mass Spectrometric Study on Low-Index Au(hkl) Surfaces. *ACS Catal.* **2019**, *9*, 1383−1388.
(34) Mezzavilla, S.; Horch, S.; Stephens, I. E. L.; Seger, B.; Chorkendorff, I. Structure Sensitivity in the Electrocatalytic Reduction of CO_2 with Gold Catalysts. *Angew. Chem., Int. Ed.* **2019**, *58*, 3774−3778.
(35) Kim, D.; Kley, C. S.; Li, Y.; Yang, P. Copper nanoparticle ensembles for selective electroreduction of CO_2 to C_2-C_3 products. *Proc. Natl. Acad. Sci. U.S.A.* **2017**, *114*, 10560−10565.
(36) Kuhl, K. P.; Cave, E. R.; Abram, D. N.; Jaramillo, T. F. New insights into the electrochemical reduction of carbon dioxide on metallic copper surfaces. *Energy Environ. Sci.* **2012**, *5*, 7050−7059.
(37) Goodpaster, J. D.; Bell, A. T.; Head-Gordon, M. Identification of Possible Pathways for C−C Bond Formation during Electrochemical Reduction of CO_2: New Theoretical Insights from an Improved Electrochemical Model. *J. Phys. Chem. Lett.* **2016**, *7*, 1471−1477.
(38) Li, F.; Li, Y. C.; Wang, Z.; Li, J.; Nam, D.-H.; Lum, Y.; Luo, M.; Wang, X.; Ozden, A.; Hung, S.-F. J. N. C. Cooperative CO2-to-ethanol conversion via enriched intermediates at molecule−metal catalyst interfaces. *Nat. Catal.* **2020**, *3*, 75−82.
(39) Wuttig, A.; Yaguchi, M.; Motobayashi, K.; Osawa, M.; Surendranath, Y. Inhibited proton transfer enhances Au-catalyzed CO_2-to-fuels selectivity. *Proc. Natl. Acad. Sci. U.S.A.* **2016**, *113*, E4585−E4593.
(40) Ross, M. B.; Dinh, C. T.; Li, Y.; Kim, D.; De Luna, P.; Sargent, E. H.; Yang, P. Tunable Cu Enrichment Enables Designer Syngas Electrosynthesis from CO_2. *J. Am. Chem. Soc.* **2017**, *139*, 9359−9363.
(41) Li, H.; Wei, P.; Gao, D.; Wang, G. In situ Raman spectroscopy studies for electrochemical CO_2 reduction over Cu catalysts. *Current Opinion in Green and Sustainable Chemistry* **2022**, *34*, 100589.
(42) Zheng, Y.; Vasileff, A.; Zhou, X.; Jiao, Y.; Jaroniec, M.; Qiao, S.-Z. Understanding the Roadmap for Electrochemical Reduction of CO_2 to Multi-Carbon Oxygenates and Hydrocarbons on Copper-Based Catalysts. *J. Am. Chem. Soc.* **2019**, *141*, 7646−7659.
(43) Zhu, C.; Zhao, S.; Shi, G.; Zhang, L. Structure-Function Correlation and Dynamic Restructuring of Cu for Highly Efficient Electrochemical CO_2 Conversion. *ChemSusChem* **2022**, *15*, e202200068.

https://doi.org/10.1021/acs.jpcc.2c08241
J. Phys. Chem. C 2023, 127, 3470−3477